PARADOXICAL IMPACT OF SPRAWLING INTRA-URBAN HEAT ISLETS: REDUCING MEAN SURFACE TEMPERATURES WHILE ENHANCING LOCAL EXTREMES

A PREPRINT

Anamika Shreevastava[1,*], **Saiprasanth Bhalachandran**[2,+], **Gavan S. McGrath**[3], **Matthew Huber**[2], and **P. Suresh C. Rao**[1]

1. Lyles School of Civil Engineering, Purdue University, West Lafayette, IN, USA
2. Department of Earth, Atmospheric, and Planetary Sciences, Purdue University, IN, USA
3. Ecosystem Science, Department of Biodiversity Conservation and Attractions, Kensington, WA, Australia
+Current affiliation: Department of Earth System Science, Stanford University, CA, USA

*Corresponding author: ashreeva@purdue.edu; `http://anamika255.github.io`

ABSTRACT

Extreme heat is one of the deadliest health hazards that is projected to increase in intensity and persistence in the near future. Here, we tackle the problem of spatially heterogeneous extreme heat distribution within urban areas. We develop a novel multi-scale metric of identifying emerging heat clusters at various percentile-based thermal thresholds and refer to them collectively as *intra-Urban Heat Islets*. Using remotely sensed Land Surface Temperatures, we first quantify the spatial organization of heat islets in cities at various degrees of sprawl and densification. We then condense the size, spacing, and intensity information about heterogeneous clusters into probability distributions that can be described using single scaling exponents (denoted by β, Λ_{score}, and λ, respectively). This allows for a seamless comparison of the heat islet characteristics across cities at varying spatial scales and improves on the traditional Surface Urban Heat Island (SUHI) Intensity as a bulk metric. Analysis of Heat Islet Size distributions demonstrates the emergence of two classes where the dense cities follow a Pareto distribution, and the sprawling cities show an exponential tempering of Pareto tail. This indicates a significantly reduced probability of encountering large heat islets for sprawling cities. In contrast, analysis of Heat Islet Intensity distributions indicate that while a sprawling configuration is favorable for reducing the mean SUHI Intensity of a city, for the same mean, it also results in higher local thermal extremes. This poses a paradox for urban designers in adopting expansion or densification as a growth trajectory to mitigate the UHI.

Introduction

More than 50% of the world's population currently resides in cities, and the number continues to increase rapidly with a projection that 70% of the global population will be urbanized by 2050 (Prudhomme, 2018). Rapid urbanization trends are manifested in expansion and densification of existing cities and the merging of agglomerations to form megacities, particularly in South Asia and sub-Saharan Africa (Seto and Shepherd, 2009). Among the numerous challenges that cities face, a particularly urgent problem due to climate change is that of extreme heat. Urban areas often raise the local temperatures relative to natural and rural surroundings leading to the phenomenon of Urban Heat Island (UHI) effect. A synergistic interaction between UHIs and increasingly persistent heat waves further exacerbates the extreme temperatures within cities (Li and Bou-Zeid, 2013; Zhao et al., 2018). Repercussions of extreme heat include thermal discomfort (Nikolopoulou and Lykoudis, 2006), increased energy consumption (Santamouris, 2014), and a greater number of heat-related casualties during heat waves (Semenza et al., 1996; Uejio et al., 2011).

The UHI is typically quantified as UHI Intensity, i.e. the difference between the air temperatures of a representative urban area (point measurement or spatial average) and rural area. However, such an estimate is inadequate to address the *intra-urban* spatial heterogeneity. Commendable efforts to collect spatially resolved thermal data such as the Basel Urban Boundary Layer Experiment (BUBBLE) campaign (Rotach et al., 2005) are rare and often limited to a single city. On the other hand, earth-monitoring satellites such as Landsat and Moderate Resolution Imaging Spectroradiometer (MODIS) enable consistent high spatial resolution characterization across multiple cities. As a result, the Surface UHI (SUHI) estimated using Land Surface Temperatures (LST) has emerged as an alternative approach which we adopt in this study (Roth et al., 1989; Voogt and Oke, 2003). For satellite sensors, urban features such as building roof and wall exteriors, surface materials, albedo, impervious and vegetated fractions, and surface moisture within each pixel determine the resultant LST. Note that while SUHI bears similarity in spatial and temporal patterns to UHI, spatial patterns of SUHI are more coupled with urban form and function, whereas air temperatures are subject to the boundary layer wind profiles as well, therefore, a point-to-point correspondence can not be expected (Panwar et al., 2019).

LST, which is strongly determined by the land use land cover properties, emerges from the underlying self-organization of the urban forms. As a result, the role of spatial organization of urban form in reducing SUHI Intensity has been a topic of substantial research spanning multitude of spatial scales. At the micro-scale, i.e. within the urban canyon, the surface temperatures are extremely sensitive to the geometrical details of immediate surroundings, such as street canyon geometry, sky-view factor, vegetative fraction, solar access and shading (Jamei et al., 2016; Taleghani et al., 2015; Andreou, 2013). However, at the local scale, i.e. of the order of few kilometers, consistent thermal patterns emerge due to locally homogeneous patches of urban form and function (Stewart and Oke, 2012; Ching et al., 2018). We do not have a clear understanding of the optimal urban form and function that minimize the urban heat locally as well as at a city-scale. For instance, studies investigating local scale impacts (Sobstyl et al., 2018; Schwarz and Manceur, 2014) report that high-density urban development leads to higher local temperatures, whereas, several others note that sprawling urban development may result in worse thermal conditions (Stone Jr and Rodgers, 2001; Stone et al., 2010). Debbage and Shepherd (2015) show that regardless of the urban density type *within a patch*, the relative spatial contiguity of the urban land use patches is a critical variable as well. Despite these recent advances on

the intra-urban thermal landscape over the last few decades, a comprehensive framework for the characterization of intra-urban thermal heterogeneity for diverse city morphologies is still lacking.

We use a multi-scale framework wherein we treat the SUHI not as a single entity, but as a collection of heterogeneous clusters of heat within the city. We refer to these clusters as **intra-urban heat islets**. The objective of this study is to evaluate the impact of spatial organization of these heat islets on their properties such as size and intensity and determine if there is a favourable spatial structure for reducing surface temperature extremes at intra-urban spatial scales. Urban morphology, and as a result LST, emerges via the processes of densification and expansion, albeit constrained by cultural, geographic and economic factors (Batty, 2013; Mustafa et al., 2018). Different degrees and combinations of these two processes result in diversity of form and function. Dense urban growth occurs when there is increased in-fill construction within existing high-density built-up area. Such a process is often driven by economic and socio-political factors that lead to settlement of new urban regions close to the city center (Andersson et al., 2006). This is akin to the preferential attachment phenomenon observed in complex networks where a new node is more likely to agglomerate at the ”hub nodes” with the highest density of edges (Barabási and Albert, 1999). We hypothesize that the densification within urban area results in hot regions getting hotter and larger thereby resulting in a heavy-tailed size distribution of heat islets. Urban expansion in the form of sprawl, on the other hand, occurs at the periphery of urban areas in the form of growing sub-urban regions. We hypothesize that this would lead to the emergence of heat islets that are spread more evenly throughout the city, often interspersed with local heat sinks. This can be detected in the size distribution as a fast decaying tail, often in the form of an exponential tempering (Amaral et al., 2000). Similar effects of urban expansion and densification on the power-law node degree observed is observed in several urban infrastructure systems such as roads and sewage networks (Mohajeri et al., 2015; Yang et al., 2017; Klinkhamer et al., 2017). Note that we don't refer to the spatial organization of urban assets such as buildings or impervious areas. Rather, we directly analyze the LST. We implement the framework for a set of 78 cities sampled globally. Using probabilistic models, we condense the size, spacing, and intensity information about heterogeneous clusters into distributions that can be described using single scaling exponents. This allows for a seamless comparison of the heat islet characteristics across cities that represent varying degrees of sprawl or densification. We then assess how the thermal spatial structure relates to the traditional lumped metric, SUHI Intensity. Lastly, we discuss implications for desirable thermal configurations for cities to minimize the area and intensity of the heat islets.

Data acquisition and Clustering technique

A set of 78 cities were sampled encompassing diverse climatological, geographical, and cultural backgrounds as well as different realizations of urban form and function (Figure 1). The cities selected range from megalopolises such as Guangzhou, London, and New York City with a population of over 10 Million and metropolitan areas up to 3000 km^2, to smaller cities such as Tbilisi, Bern, and Oslo that span less than 100 km^2. As a globally standardized dataset of urban extent, the Urban Land Use layer of Land Cover product from MODIS was used. The exact definition of urban boundaries and city area plays a significant role in urban scaling laws (Cottineau et al., 2017), therefore, a buffer of 5 km in the rural regions was taken to account for the peri-urban settlements. However, as the heat islets occur well within the city boundaries, the results were found to be independent of the buffer width.

For each city, we selected a Landsat image of a summertime cloud-free day, and derived the LST in the geospatial computing environment of Google Earth Engine (Gorelick et al., 2017) using the methodology described in Walawender et al. (2012) (Walawender et al., 2012). A novel aspect of our methodology is the clustering technique used to characterize the LST. The LSTs are treated analogously to topography in Digital Elevation Models (DEM), where the temperatures substitute for elevation (Shreevastava et al., 2018). As the cities belong to diverse climatic backgrounds (and hence, background temperatures) (Zhao et al., 2014), percentile-based thermal thresholds were chosen for identifying the relative hottest regions within the urban areas. The areas above a given thermal threshold (e.g., corresponding to percentiles of temperatures) were identified, and the connected pixels were grouped into a cluster that we refer to as a **heat islet**. Supplementary Information provides code and text describing the methods in more detail.

Size distribution of heat islets

In an exploration of *shapes* of heat islets, we found consistent self-similar, fractal topography across all cities (Shreevastava et al., 2019) (See Supplementary Figure 1). Here, we focus on their *size* distribution by building on the scaling laws known for fractal surfaces. According to Korcak's law, the size distribution of clusters in a fractal topography is expected to follow a power law at the percolation threshold (Imre and Novotnỳ, 2016; Mandelbrot, 1975; Isichenko and Kalda, 1991). This is mathematically represented as: $N(a) \propto a^{-\beta}$ where N is the number of clusters of area, a, and the scaling exponent is β. Expressed as an exceedance probability we can write it as a Pareto distribution:

$$P(A \geq a) \propto a^{1-\beta}, \quad \forall\, a \geq a_{min} \tag{1}$$

where, for a given area a, the probability of an islet having an area A larger than a is represented by P, the scaling exponent is represented by β, and the minimum area at or above which the power-law is valid is represented as a_{min}. We use Maximum Likelihood Estimation (MLE) to test for and fit the exceedance probability distributions(Clauset et al., 2009) (See Supplementary Text 3). This process is carried out for multiple thermal thresholds (50^{th}, 60^{th}, $\cdots$, 90^{th} percentiles). We find that the estimated exponents ranged between 1.6 to 2.2 with a mean $\beta = 1.88$. However, for the smaller cities ($A_{city} \leq 650$ km^2), the variability in exponents was much larger (Supplementary Figure 2). One explanation for this is statistical, wherein for small cities there are not enough islets obtained at 90 m resolution which results higher statistical fluctuations about the mean are observed. As the number of islets increases with city size, steady averaging is achieved that results in convergence towards the mean. However, from an urban growth perspective, this behavior is consistent with several other complex systems that operate within cities (Klinkhamer et al., 2017; Barthelemy, 2016). For smaller cities, the variability due to factors unrelated to city size result in more detectable fluctuations and it simply indicates that they have not grown in size enough to display self-organization yet (Batty, 2008). We, therefore, excluded those from any further analysis and proceed with 49 cities where the internal thermal structure could be reliably quantified. For the larger cities, the distributions were well described by Equation 1 with the same mean exponent and a narrow variability (std. dev. = 0.026).

The impact of a dense or sprawling spatial organization becomes apparent in how the exceedance probability distributions change as the threshold increases. The large metropolitan regions of Lagos and Jakarta are selected as

representatives of dense cities, where Chicago and Guangzhou are chosen to represent sprawling cities (Figure 2a,b). The Pareto size distribution is consistent at lower thresholds for all cities. At 90th percentile threshold, however, Lagos and Jakarta show a pronounced aggregation of heat islets indicative of dominance of a dense urban center, whereas Chicago and Guangzhou are more dispersed (Figure 2c,d). In agreement with our initial hypothesis, Lagos and Jakarta, display a Pareto heat islet size distribution across all the thresholds (Figure 2e). However, for Chicago and Guangzhou, the heat islet size distributions deviate significantly from the Pareto in the form of an exponential tempering (Figure 2f), such that their distributions more closely follow:

$$P(A \geq a) \propto a^{1-\beta} \cdot e^{-c \cdot a}, \quad \forall\, a \geq a_{min} \tag{2}$$

where c represents the exponential tempering coefficient (Supplementary Table 3).

Such behavior is explained by invoking percolation theory (Isichenko, 1992; Sahimi and Sahimi, 2014). Percolation theory is the study of random clusters and their spatial connectivity at a given threshold. The coagulation of dispersed clusters into a contiguous component is referred to as percolation, and the largest cluster is identified as the percolating cluster. In fractal landscapes, the Pareto size distribution of clusters holds within a finite range (Percolation Transition Range) of thresholds, i.e., until the percolating cluster retains its identity. We computed the percolation transition range by identifying the inflection points in the size of the largest cluster as a function of temperature threshold (Figure 2g,h). The range was then normalized using the minimum and maximum temperatures for each city such that the range is restricted to 0 and 1. We refer to this as the Normalized Percolation Range (NPR) (Supplementary Figure 3). In case of the aggregated cities (e.g. Jakarta and Lagos) as the temperature threshold is increased, the largest connected islet decreases in size gradually, and the resulting NPR is large (Figure 2g). Conversely, in the case of sprawling cities (e.g., Chicago and Guangzhou) there is a much sharper decrease in the size of the percolating cluster (Figure 2h) resulting in a narrow NPR (Figure 2i,j). As the 90th percentile thresholds in these cases fall outside the NPR (Figure 2j), exponential tempering is observed.

From the perspective of the size distribution of heat islets alone, as the thermal threshold is increased, fewer and smaller heat islets are captured. Therefore, an exponential tempering presents a reduced probability of encountering large heat islets of higher temperatures. This suggests that a sprawling spatial structure is favourable for reducing the size of extreme heat islets. Thus far, we have characterized the size distribution of these islets, not their spatial organization. We now introduce a metric to quantify and analyze the relationship between the spacing of the urban heat islets and the characteristics we observed in their size distributions.

Quantifying Aggregated vs Dispersed heat islets: Lacunarity

A built-up patch in a city acts as a source of increased sensible heat flux, as well as anthropogenic heat flux due to human activities such as air-conditioning. Likewise, the gaps between the patches (also referred to as spacing in this work), often water or vegetation, act as heat sinks that absorb the excess heat generated. Therefore, characterizing this spacing between the urban patches is an essential step towards ameliorating heat stress (Debbage and Shepherd, 2015). Particularly, the impact of the relative sizes and strengths of such sources and sinks on the overall thermal landscape

has been relatively understudied and requires further investigation. Since the present study focuses on the thermal landscape characterized by LST, we can directly quantify the spacing between the identified heat islets. Popular metrics such as root mean square distances work well for Gaussian systems, but for fractal landscapes, lacunarity is a better-suited metric of spatial structure (Plotnick et al., 1996). Lacunarity (Λ) is a scale-dependent measure of the aggregation of spaces between the heat islets (Mandelbrot, 1982; Plotnick et al., 1996). A 'gliding box' algorithm for the calculation of Λ as a function of box size (r), as described in Plotnick et al. (1993), was adopted here (Methods section). While the absolute values of Λ offer little insight, the appropriate way to interpret lacunarity is in the context of the rate of change of Λ as a function of r. If the value of $log(\Lambda(r))$ decreases at any scale (quantified with $log(r)$), the presence of spacing corresponding to that length scale is indicated. The two extremes of lacunarity curvature can be best conceptualized as a chessboard-type homogeneous distribution of small-scale spacing, and a single contiguous cluster. Essentially, the length scales corresponding the steepest slopes should be interpreted as the dominant scale of spacing.

As the differences in the spatial organization of heat islets are most apparent at higher temperature thresholds, here, we characterized the spatial structure obtained at the 90$^{\text{th}}$ percentile of LST for all cities. By extension, the total *islet area* under consideration corresponds to the hottest 10% of the total city area. Lacunarity curves for the four representative cities investigated in the previous section are highlighted in Figure 3. The cities that have a dominance of larger spacing between the islets lay above the diagonal. Conversely, a dispersed spatial structure of the heat islets manifests as smaller spacing, fall under the diagonal. We assign a single score (Λ_{score}) to the convexity of the curves in Figure 3a such that positive scores indicate larger spacing and vice-versa. This is achieved using the following empirical equation:

$$log_{10}\big(\Lambda(r)\big) = \left(1 - \frac{log_{10}(r)}{2}\right)^{2^{\Lambda_{score}}} \tag{3}$$

where constants 1 and 2 are used to fix the end points of the curve at $log(\Lambda(r)) = 1$ and $log(r) = 2$, and the exponent, Λ_{score} is scale-independent measure of the shape of the lacunarity curve (See Methods section). The 49 cities have Λ_{score} ranging between -0.9 to 0.6, and distributed normally (Figure 3b; See Supplementary Table 4).

Using Λ_{score}, we compare the relationship between the islet spacing and their NPR (and by extension, likely exponential tempering at higher thresholds). We find that the dense cities associated with an aggregated heat islet structure (positive Λ_{score}) display a larger NPR (≥ 0.25; Figure 3c). Whereas, sprawling and disaggregated cities (negative Λ_{score}) have a smaller NPR (< 0.25; Figure 3c) and consequently an exponential tempering of the power law tail (Figure 2f). An exception to this pattern are cities with a negative Λ_{score} despite having an NPR ≥ 0.25 (shown in yellow in Figure 3c). Upon examination, we found these to have a significant river flowing right through them. Under such a scenario, the percolating heat cluster is divided structurally into two halves by a heat sink, irrespective of the threshold (Supplementary Figure 4). This results in a negative Λ_{score} due to the spacing introduced by the river despite an aggregation of heat islets on either side of the river. Thus, Figure 3c serves to quantitatively affirm the correlation between the spatial configuration of cities (dense and/or sprawling) and the 2 classes of size distributions of the heat islets.

Note that for any given size distribution, the islets can be spatially arranged in several ways. In order to examine the variability in islet size and spacing of the various cities, we define two scale-independent metrics to characterize size: Mean (A_M) and Largest (A_L) Relative Heat Islet Sizes, calculated as a percentage of the total city area. First, we observe that there is a weak positive correlation ($R^2 = 0.4$) between A_M and spacing of the heat-islets (Figure 3d). This is expected because a positive Λ_{score} as well as a high A_M corresponds to dense cities, and a negative Λ_{score} and low A_M corresponds to sprawling cities. More noteworthy is the horizontal spread about the diagonal in Figure 3d which reflects the different spatial configurations (characterized by Λ_{score}) that are possible for any given size distribution. This spread may be explained by A_L, which increases with Λ_{score} (illustrated using marker size in Figure 3d; Supplementary Figure 5). In the bottom-left, both A_M and A_L are small. This is because negative Λ_{score} corresponds to sprawling cities where large clusters were absent in the islet-size distribution (as inferred from the exponential tempering of Pareto). In the bottom-right, however, the dominance of the largest aggregated islet results in a positive Λ_{score} despite a low A_M value. A schematic diagram drawn to represent each of the vertices of this plot is given as Supplementary Figure 6. The phase plot of A_M and Λ_{score} may be useful for city planners to gauge the current spatial structure of the thermal landscape of their cities and to determine mitigation strategies to achieve a more desirable state.

Islet Intensity distribution

Apart from the size and spacing of heat islets, we now focus on the temperatures obtained within the heat islets. To address this, we first use the well-known indicator of excess heat in urban areas, the SUHI Intensity in the traditional sense i.e., the difference between the mean urban and rural temperatures (Schwarz et al., 2011) to evaluate the average excess heat within cities. We find that larger Λ_{score} values (representative of aggregated heat islets) tend to be associated with higher SUHI Intensity (Figure 4b). This suggests that sprawling cities, with a larger number of heat sinks to match the heat sources, are a better configuration for reducing the *overall* SUHI Intensity. This is in agreement with our findings based on the size distribution of extreme heat islets as well as Debbage and Shephard (2015) findings based on discontiguity of urban patches calculated using National Land Cover Dataset (NLCD) (Debbage and Shepherd, 2015). Traditional estimates of the UHI Intensity that simply use the difference between the **mean** temperatures over an urban area and the surrounding non-urban environment fail to address the intra-urban heterogeneity adequately.

For a more comprehensive assessment of the thermal variability within cities, we introduce a novel *Heat Islet Intensity* distribution metric. First, we compute the excess heat (ΔT) for each islet as the difference between the mean *islet* temperature and the *threshold* temperature. We refer to this term as the *Islet Intensity*. We find that the mean and standard deviation of ΔT were equal (Supplementary Figure 7) which, along with the shape of its distribution (Figure 4a), were indicative that ΔT is exponentially distributed, i.e:

$$P(\Delta T \geq x) \propto 1 - e^{-\lambda x} \tag{4}$$

where, for a given islet intensity x, the probability of an islet having a temperature ΔT larger than x is represented by P, an exponential distribution characterized by λ. By extension, $1/\lambda$ is the mean islet intensity. Lower values of

λ correspond to an increased probability of higher temperatures within the islets. Therefore, a single metric, λ can be used as an indicator to capture the intra-urban thermal variability across islets. This is represented as the color bar in Figure 4b.

We find that while cities with a higher degree of sprawl have a lower mean temperature, for the same SUHI (Y-axis in Figure 4b), cities with lower Λ_{score} also experience higher likelihood of encountering thermal extremes. For example, dense cities such as Lagos and Jakarta have a steeper exponential decaying rate than Chicago and Guangzhou, which drastically reduces the probability of local thermal extremes within their heat islets. While the probability of a heat islet being hotter than the mean by 1°C is almost zero for the first two, the likelihood increases to roughly 20% for the latter two (Figure 4a). As the larger heat islets are often associated with the highest islet intensity as well, this can result in a significantly large areas of extreme heat especially for megacities like Guangzhou and Chicago. Such a finding reveals that while mean SUHI Intensity decreases with sprawling cities, for the same mean, they also experience higher local thermal extremes. As a result, in addition to the mean SUHI Intensity, it is essential to characterize the thermal heterogeneity within the cities, and the islet intensity distribution can be adopted as a complementary metric.

Summary and Conclusions

Cities grow through a combination of parallel and sequential episodes of expansion and densification at different rates. Depending on local preferences and constraints, neighborhoods are built with different spatial patterns, for example, from dense downtowns to sprawling suburbs. Factors like geographical topography, coastline, and intra-urban commuting time constrain expansion, whereas other factors such as local building laws limit densification. While there are several objective functions such as commuting travel time distribution, net carbon emissions, and socio-economical factors which urban form and functions are optimized for, here, we focus on the aspect of urban heat. More specifically, the spatial heterogeneity of extreme heat islets within urban areas. Towards that, we present a novel multi-scale framework that allows us to identify intra-urban heat islets for several thermal thresholds. Using this framework, we evaluate the impact of spatial organization, characterized by a Lacunarity-based metric, Λ_{score}. We do not find a bi-modal distribution of Λ_{score} corresponding to the two classes of sprawl or dense cities. Rather, the Λ_{score} was normally distributed around a mean value close to zero indicating that most cities display a balance between sprawl and dense heat islet structure. Different realizations and degrees of expansion and densification yield a diverse array of spatial structures.

We condense the size, spacing, and intensity information about heterogeneous clusters into probabilistic distributions that can be described using single scaling exponents. This allows for a seamless comparison of the intra-urban heat islet characteristics across cities at several spatial scales ranging from 90 meters (resolution of Landsat 8 and corresponding to several urban blocks) up to few thousand sq. km (total area of large cities). We implement this framework for 78 globally representative cities to answer the following key questions. First, how many and how big are the emergent heat islets at multiple thermal thresholds? Second, how much hotter than the threshold are these heat islets? From the size distribution analysis, we demonstrate that islet sizes in dense cities follow and maintain a power law tail across all temperature thresholds, whereas the sprawling cities show an exponential tempering of tails at higher thresholds. Such a tempering is favourable as it indicates a reduced emergence of large heat islets in

sprawling and dispersed spatial configurations. Additionally, a dispersed configurations results in lower *mean SUHI Intensity* over the city. However, from the islet intensity distribution analysis, we find that heat islet intensities (ΔT) can be modelled as exponential distributions, where dispersed configurations result in higher rate parameters, λ. This implies a significantly higher probability of encountering extreme temperatures within the islets. As a result, while a sprawling configuration is favorable for reducing the mean temperature of a city, for the same mean SUHI intensity, it results in higher local thermal extremes. The implications of this from a design perspective are that: (i) while designing sprawling cities, higher intra-urban variability should be expected. (ii) With changes in urban morphology, we can attempt to control the precise spatial location of the extreme temperatures. It is of utmost importance that the spatial locations of these extremities do not coincide with the high risk zones where most vulnerable populations reside, such as densely populated downtowns, or areas without access to air-conditioning such as urban slums.

At this juncture, we reiterate that while the spatial characterization of temperature is informative for urban heat assessments, it does not inform the overall risk to the concerned population. Risk is a combination of hazard (i.e. extreme heat-stress in this case, a combination of air temperature and humidity (Oleson et al., 2015)), the time period of exposure to heat stress, and vulnerability. Prior research shows that in the absence of hydrological processes, the changes in radiative flux, determined by LST, contribute more to the near-surface temperature changes than the turbulent heat flux (Brownlee et al., 2017). As a result, similar spatial patterns of heat islets derived from air temperatures can be expected. Vulnerability assessments will require further consideration of demographic factors such as old age, low educational attainment, high poverty levels, poor health, and lack of air conditioning (Cutter et al., 2009; Uejio et al., 2011; Bradford et al., 2015). An investigation of the spatio-temporal dynamics of risk to extreme heat is beyond the scope of the present study but it certainly warrants further research.

Lastly, our analysis here is limited to the structural heterogeneity of heat sources and sinks, and not the functional heterogeneity. If we assume a uniform heat capacity of land use, the sizes of heat islets are then indicative of the strength of the sources, and the length-scale of spacing is indicative of the sink strengths. Consideration of the *functional* heterogeneity will require a treatment of the variability in heat capacities and thermal conductivities of the land use which jointly determine heat dissipation from sources, which is possible using models such as Weather Research Forecast (WRF) (Chen et al., 2011; Salamanca et al., 2011). In such a scenario, instead of LST, heat fluxes can be treated as DEM for such an analysis. It may also then be beneficial to study the spatial correlation between source strength and sink strength to evaluate thermal dissipation. To conclude, our work presents the first steps toward a multi-scale characterization of the complex intra-urban thermal landscape and we hope that it opens new vistas for future investigations.

Methods

Study area and data sources

Land surface temperature (LST) data was derived using a Single Channel Algorithm as detailed in (Walawender et al., 2012) from Landsat 8 at a resolution of 90 m. The geo-spatial analysis environment of Google Earth Engine (GEE) was used to filter out cloud free summer time days with an incident solar angle of at least 60 degrees (Gorelick et al.,

2017). See Supplementary Text S1 and S2 for algorithms, and Table S1 for list of cities and information on Landsat scenes used. For coastal cities the Large Scale International Boundary (LSIB) dataset provided by United States Office of the Geographer was used to crop out the oceans and delineate urban boundaries within GEE environment. Urban area was estimated using MODIS's Land Cover Type dataset - MCD12Q1.

Statistical modelling of size and intensity distributions

For fitting probability distribution functions (pdfs) to cluster size and intensity distributions, a combination of maximum-likelihood estimation (mle) with goodness-of-fit tests based on the Kolmogorov-Smirnov (KS) statistic and likelihood ratios were used (Clauset et al., 2009). See Supplementary Text S3 for details and Table S2 for results.

Lacunarity

First, the landscape was sliced at a thermal threshold and an islets map was obtained. For each box size ($1 < r < A_{city}$), the number of occupied pixels (islets) was measured. The number of occupied sites was referred to as the box mass. The box was then moved one column to the right and the box mass was again counted. This process was repeated over all rows and columns producing a frequency distribution of the box masses. The number of boxes of size r containing S occupied sites was designated by n(S,r) and the total number of boxes of size r by N(r). This frequency distribution was converted into a probability distribution: $Q(S,r) = \frac{n(S,r)}{N(r)}$. Lacunarity was a measure of variability in the calculated occupancy for each box size.

$$\Lambda(r) = \frac{VarianceQ(S,r)}{MeanQ(S,r)^2} + 1 \tag{5}$$

For all cities, Lacunarity score was calculated only for the 90$^{\text{th}}$ percentile thermal threshold. As a result, 90% of the total area in all cases comprised of spaces and the $\Lambda(r)$ value for box size = 1 was the same for all cities. The largest box size taken under consideration is normalized from 0 to 100 in order to account for the variable sizes of cities. Note that the curvature of Lacunarity curve was unaffected by these transformations.

Acknowledgments

The authors thank the organizers and participants of a series of Complex Networks Synthesis workshops; co-hosted by Purdue University, University of Florida, Helmholtz Centre for Environmental Research, UFZ, and Technical University, Dresden, Germany; for creating a trans-disciplinary collaborative research environment and providing critical input across multiple workshops. The authors appreciate the discussions on lacunarity with Prof. Joaquín C. Goñi. A.S. and S.B. gratefully acknowledge the financial support from NASA in the form of their NASA Earth and Space Science Fellowships (Grant numbers: 80NSSC17K0441 and NNX15AM72H, respectively). P.S.C.R. acknowledges the support from NSF Collaborative Research - RIPS Type 2: Resilience Simulation for Water, Power and Road Networks (1441188) and the Lee A. Reith Endowment in the Lyles School of Civil Engineering at Purdue University.

References

Amaral, L. A. N., A. Scala, M. Barthelemy, and H. E. Stanley, 2000: Classes of small-world networks. *Proceedings of the national academy of sciences*, **97 (21)**, 11 149–11 152.

Andersson, C., K. Frenken, and A. Hellervik, 2006: A complex network approach to urban growth. *Environment and Planning A*, **38 (10)**, 1941–1964.

Andreou, E., 2013: Thermal comfort in outdoor spaces and urban canyon microclimate. *Renewable Energy*, **55**, 182–188.

Barabási, A.-L., and R. Albert, 1999: Emergence of scaling in random networks. *science*, **286 (5439)**, 509–512.

Barthelemy, M., 2016: *The structure and dynamics of cities*. Cambridge University Press.

Batty, M., 2008: The size, scale, and shape of cities. *science*, **319 (5864)**, 769–771.

Batty, M., 2013: *The new science of cities*. Mit Press.

Bradford, K., L. Abrahams, M. Hegglin, and K. Klima, 2015: A heat vulnerability index and adaptation solutions for pittsburgh, pennsylvania. *Environmental Science & Technology*, **49 (19)**, 11 303–11 311.

Brownlee, J., P. Ray, M. Tewari, and H. Tan, 2017: Relative role of turbulent and radiative flux on the near-surface temperature in a single-layer urban canopy model over houston. *Journal of Applied Meteorology and Climatology*, **56 (8)**, 2173–2187.

Chen, F., and Coauthors, 2011: The integrated wrf/urban modelling system: development, evaluation, and applications to urban environmental problems. *International Journal of Climatology*, **31 (2)**, 273–288.

Ching, J., and Coauthors, 2018: Wudapt: An urban weather, climate, and environmental modeling infrastructure for the anthropocene. *Bulletin of the American Meteorological Society*, **99 (9)**, 1907–1924.

Clauset, A., C. R. Shalizi, and M. E. Newman, 2009: Power-law distributions in empirical data. *SIAM Review*, **51 (4)**, 661–703.

Cottineau, C., E. Hatna, E. Arcaute, and M. Batty, 2017: Diverse cities or the systematic paradox of urban scaling laws. *Computers, environment and urban systems*, **63**, 80–94.

Cutter, S. L., C. T. Emrich, J. J. Webb, and D. Morath, 2009: Social vulnerability to climate variability hazards: A review of the literature. *Final Report to Oxfam America*, **5**, 1–44.

Debbage, N., and J. M. Shepherd, 2015: The urban heat island effect and city contiguity. *Computers, Environment and Urban Systems*, **54**, 181–194.

Gorelick, N., M. Hancher, M. Dixon, S. Ilyushchenko, D. Thau, and R. Moore, 2017: Google earth engine: Planetary-scale geospatial analysis for everyone. *Remote Sensing of Environment*, **202**, 18–27.

Imre, A. R., and J. Novotnỳ, 2016: Fractals and the korcak-law: a history and a correction. *The European Physical Journal H*, **41 (1)**, 69–91.

Isichenko, M., and J. Kalda, 1991: Statistical topography. i. fractal dimension of coastlines and number-area rule for islands. *Journal of Nonlinear Science*, **1 (3)**, 255–277.

Isichenko, M. B., 1992: Percolation, statistical topography, and transport in random media. *Reviews of Modern Physics*, **64 (4)**, 961.

Jamei, E., P. Rajagopalan, M. Seyedmahmoudian, and Y. Jamei, 2016: Review on the impact of urban geometry and pedestrian level greening on outdoor thermal comfort. *Renewable and Sustainable Energy Reviews*, **54**, 1002–1017.

Klinkhamer, C., E. Krueger, X. Zhan, F. Blumensaat, S. Ukkusuri, and P. S. C. Rao, 2017: Functionally fractal urban networks: Geospatial co-location and homogeneity of infrastructure. *arXiv preprint arXiv:1712.03883*.

Li, D., and E. Bou-Zeid, 2013: Synergistic interactions between urban heat islands and heat waves: the impact in cities is larger than the sum of its parts. *Journal of Applied Meteorology and Climatology*, **52 (9)**, 2051–2064.

Mandelbrot, B. B., 1975: Stochastic models for the earth's relief, the shape and the fractal dimension of the coastlines, and the number-area rule for islands. *Proceedings of the National Academy of Sciences*, **72 (10)**, 3825–3828.

Mandelbrot, B. B., 1982: *The fractal geometry of nature*, Vol. 2. WH freeman New York.

Mohajeri, N., A. Gudmundsson, and J.-L. Scartezzini, 2015: Expansion and densification of cities: linking urban form to ecology. *Proceedings of International Conference CISBAT 2015 Future Buildings and Districts Sustainability from Nano to Urban Scale*, LESO-PB, EPFL, 475–480, CONF.

Mustafa, A., A. Heppenstall, H. Omrani, I. Saadi, M. Cools, and J. Teller, 2018: Modelling built-up expansion and densification with multinomial logistic regression, cellular automata and genetic algorithm. *Computers, Environment and Urban Systems*, **67**, 147–156.

Nikolopoulou, M., and S. Lykoudis, 2006: Thermal comfort in outdoor urban spaces: analysis across different european countries. *Building and environment*, **41 (11)**, 1455–1470.

Oleson, K., A. Monaghan, O. Wilhelmi, M. Barlage, N. Brunsell, J. Feddema, L. Hu, and D. Steinhoff, 2015: Interactions between urbanization, heat stress, and climate change. *Climatic Change*, **129 (3-4)**, 525–541.

Panwar, A., A. Kleidon, and M. Renner, 2019: Do surface and air temperatures contain similar imprints of evaporative conditions? *Geophysical Research Letters*.

Peel, M. C., B. L. Finlayson, and T. A. McMahon, 2007: Updated world map of the köppen-geiger climate classification. *Hydrology and Earth System Sciences*, **4 (2)**, 439–473.

Plotnick, R. E., R. H. Gardner, W. W. Hargrove, K. Prestegaard, and M. Perlmutter, 1996: Lacunarity analysis: a general technique for the analysis of spatial patterns. *Physical review E*, **53 (5)**, 5461.

Plotnick, R. E., R. H. Gardner, and R. V. O'Neill, 1993: Lacunarity indices as measures of landscape texture. *Landscape ecology*, **8 (3)**, 201–211.

Prudhomme, M., 2018: World urbanization prospects: The 2018 revision. *UN Department of Public Information*, available online: https://www.un.org/development/desa/en/news/population/2018-revision-of-world-urbanization-prospects.html.

Rotach, M., and Coauthors, 2005: Bubble–an urban boundary layer meteorology project. *Theoretical and Applied Climatology*, **81 (3-4)**, 231–261.

Roth, M., T. Oke, and W. Emery, 1989: Satellite-derived urban heat islands from three coastal cities and the utilization of such data in urban climatology. *International Journal of Remote Sensing*, **10 (11)**, 1699–1720.

Sahimi, M., and M. Sahimi, 2014: *Applications of percolation theory*. CRC Press.

Salamanca, F., A. Martilli, M. Tewari, and F. Chen, 2011: A study of the urban boundary layer using different urban parameterizations and high-resolution urban canopy parameters with wrf. *Journal of Applied Meteorology and Climatology*, **50 (5)**, 1107–1128.

Santamouris, M., 2014: On the energy impact of urban heat island and global warming on buildings. *Energy and Buildings*, **82**, 100–113.

Schwarz, N., S. Lautenbach, and R. Seppelt, 2011: Exploring indicators for quantifying surface urban heat islands of european cities with modis land surface temperatures. *Remote Sensing of Environment*, **115 (12)**, 3175–3186.

Schwarz, N., and A. M. Manceur, 2014: Analyzing the influence of urban forms on surface urban heat islands in europe. *Journal of Urban Planning and Development*, **141 (3)**, A4014 003.

Semenza, J. C., C. H. Rubin, K. H. Falter, J. D. Selanikio, W. D. Flanders, H. L. Howe, and J. L. Wilhelm, 1996: Heat-related deaths during the july 1995 heat wave in chicago. *New England Journal of Medicine*, **335 (2)**, 84–90.

Seto, K. C., and J. M. Shepherd, 2009: Global urban land-use trends and climate impacts. *Current Opinion in Environmental Sustainability*, **1 (1)**, 89–95.

Shreevastava, A., P. S. C. Rao, and G. McGrath, 2019: Emergent self-similarity and scaling properties of fractal intra-urban heat islets for diverse global cities. *EarthArXiv*, doi:10.31223/osf.io/t9s3g, URL https://eartharxiv.org/t9s3g/.

Shreevastava, A., P. S. C. Rao, and G. S. McGrath, 2018: Spatial analysis of the surface urban heat island. *Land Surface and Cryosphere Remote Sensing IV*, International Society for Optics and Photonics, Vol. 10777, 107770C.

Sobstyl, J., T. Emig, M. A. Qomi, F.-J. Ulm, and R.-M. Pellenq, 2018: Role of city texture in urban heat islands at nighttime. *Physical review letters*, **120 (10)**, 108 701.

Stewart, I. D., and T. R. Oke, 2012: Local climate zones for urban temperature studies. *Bulletin of the American Meteorological Society*, **93 (12)**, 1879–1900.

Stone, B., J. J. Hess, and H. Frumkin, 2010: Urban form and extreme heat events: are sprawling cities more vulnerable to climate change than compact cities? *Environmental health perspectives*, **118 (10)**, 1425.

Stone Jr, B., and M. O. Rodgers, 2001: Urban form and thermal efficiency: how the design of cities influences the urban heat island effect. *American Planning Association. Journal of the American Planning Association*, **67 (2)**, 186.

Taleghani, M., L. Kleerekoper, M. Tenpierik, and A. van den Dobbelsteen, 2015: Outdoor thermal comfort within five different urban forms in the netherlands. *Building and environment*, **83**, 65–78.

Uejio, C. K., O. V. Wilhelmi, J. S. Golden, D. M. Mills, S. P. Gulino, and J. P. Samenow, 2011: Intra-urban societal vulnerability to extreme heat: the role of heat exposure and the built environment, socioeconomics, and neighborhood stability. *Health & Place*, **17 (2)**, 498–507.

Voogt, J. A., and T. R. Oke, 2003: Thermal remote sensing of urban climates. *Remote Sensing of Environment*, **86 (3)**, 370–384.

Walawender, J. P., M. J. Hajto, and P. Iwaniuk, 2012: A new arcgis toolset for automated mapping of land surface temperature with the use of landsat satellite data. *Geoscience and Remote Sensing Symposium (IGARSS), 2012 IEEE International*, IEEE, 4371–4374.

Yang, S., K. Paik, G. S. McGrath, C. Urich, E. Krueger, P. Kumar, and P. S. C. Rao, 2017: Functional topology of evolving urban drainage networks. *Water Resources Research*, **53 (11)**, 8966–8979.

Zhao, L., X. Lee, R. B. Smith, and K. Oleson, 2014: Strong contributions of local background climate to urban heat islands. *Nature*, **511 (7508)**, 216.

Zhao, L., M. Oppenheimer, Q. Zhu, J. W. Baldwin, K. L. Ebi, E. Bou-Zeid, K. Guan, and X. Liu, 2018: Interactions between urban heat islands and heat waves. *Environmental research letters*, **13 (3)**, 034 003.

Figures

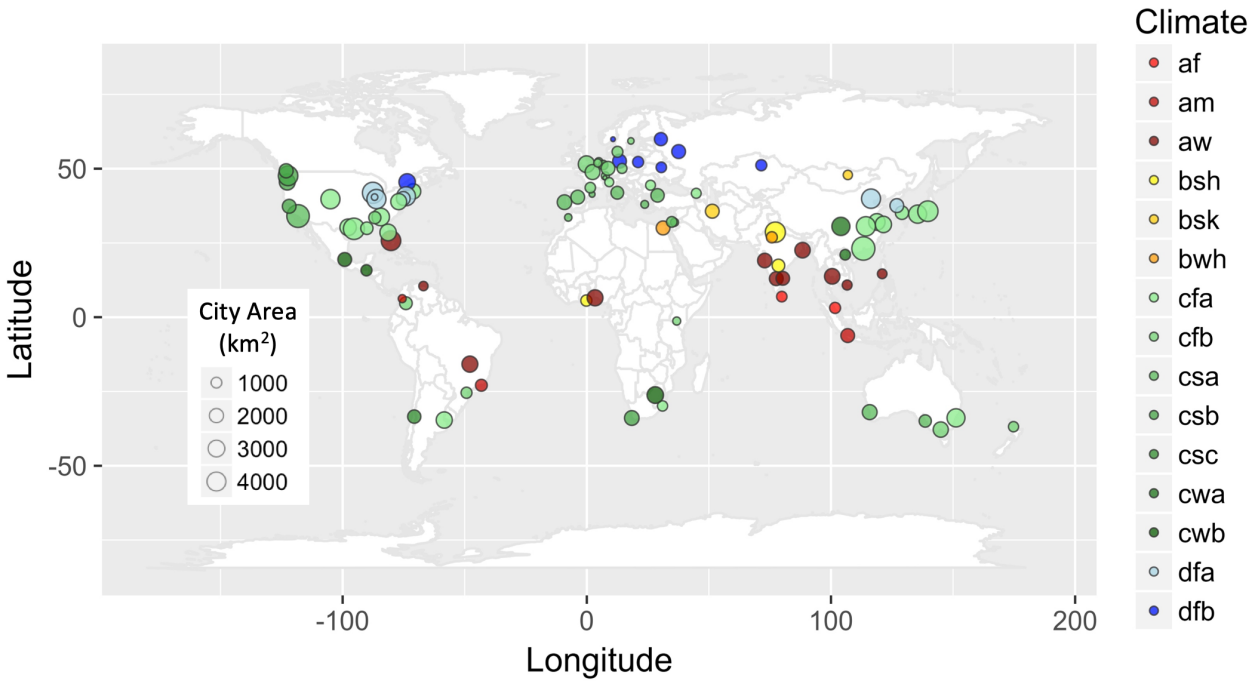

Figure 1: World map showing the locations of 78 cities considered in this study. The marker size is representative of the city size, and the colour represents their Koppen-Geiger climate classification Peel et al. (2007). Description of Koppen-Geiger climate types are given in Supplementary Table 1.

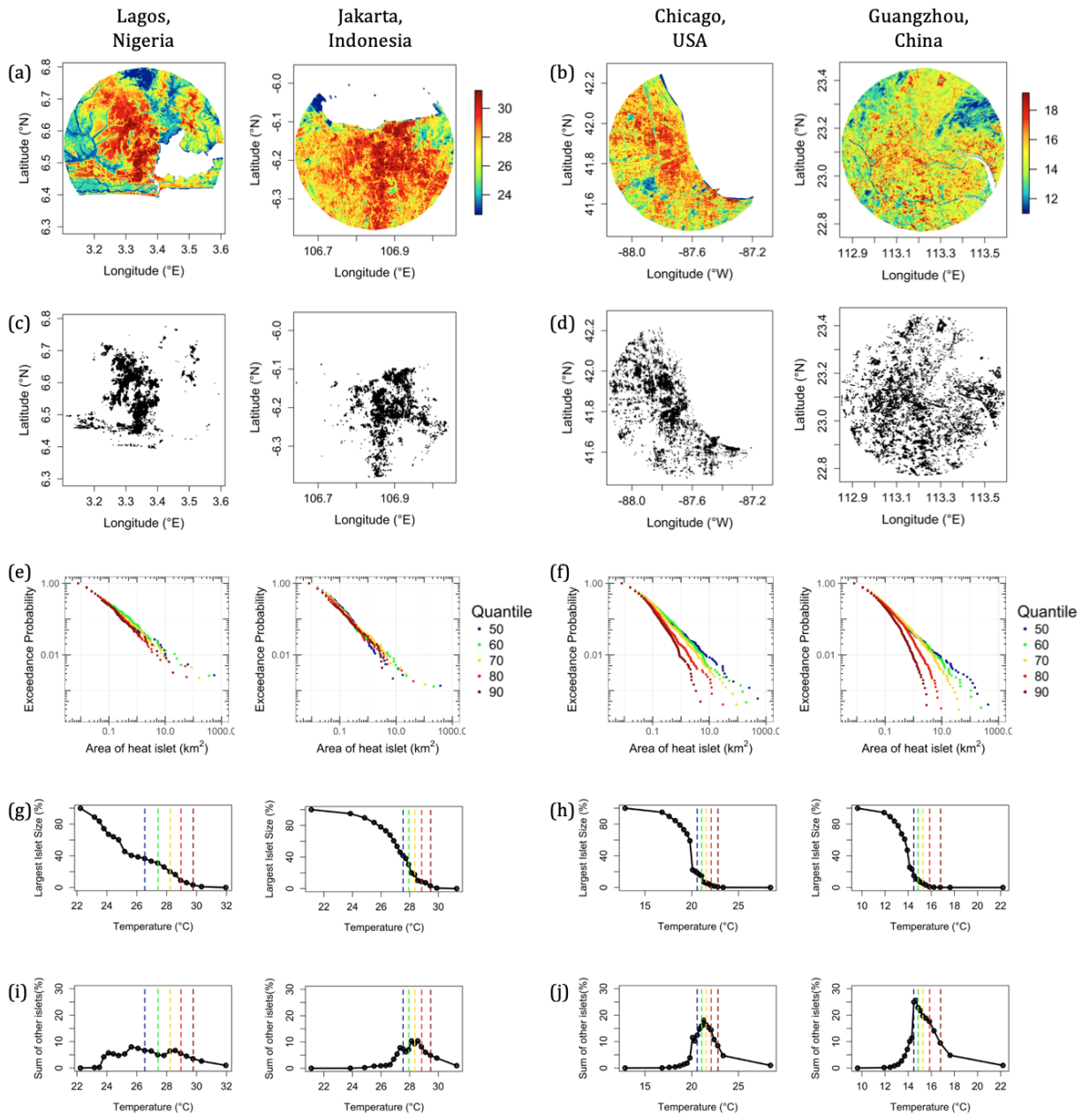

Figure 2: Two groups of cities emerge based on the size distributions of heat islets at incremental thermal thresholds. Two representative cities for each group - Jakarta, Indonesia and Lagos, Nigeria for dense cities, and Chicago, USA, and Guangzhou, China for sprawling cities - are shown. (a,b) Land Surface Temperature map (in °C), (c,d) Heat islets that emerge at the 90^{th} percentile thermal threshold, (e,f) Exceedance probability plots for heat islets at several thermal thresholds (50^{th}, $\cdots$, 90^{th}). Note the leftward shift in size distribution as the thresholds increase, especially the exponential tempering evident in sprawling cities, (g,h) Largest islet size, and (i,j) sum of remaining islets (as a % of total city area), as a function of thermal threshold. The vertical dashed coloured lines mark the temperatures corresponding to the percentiles used in (e,f).

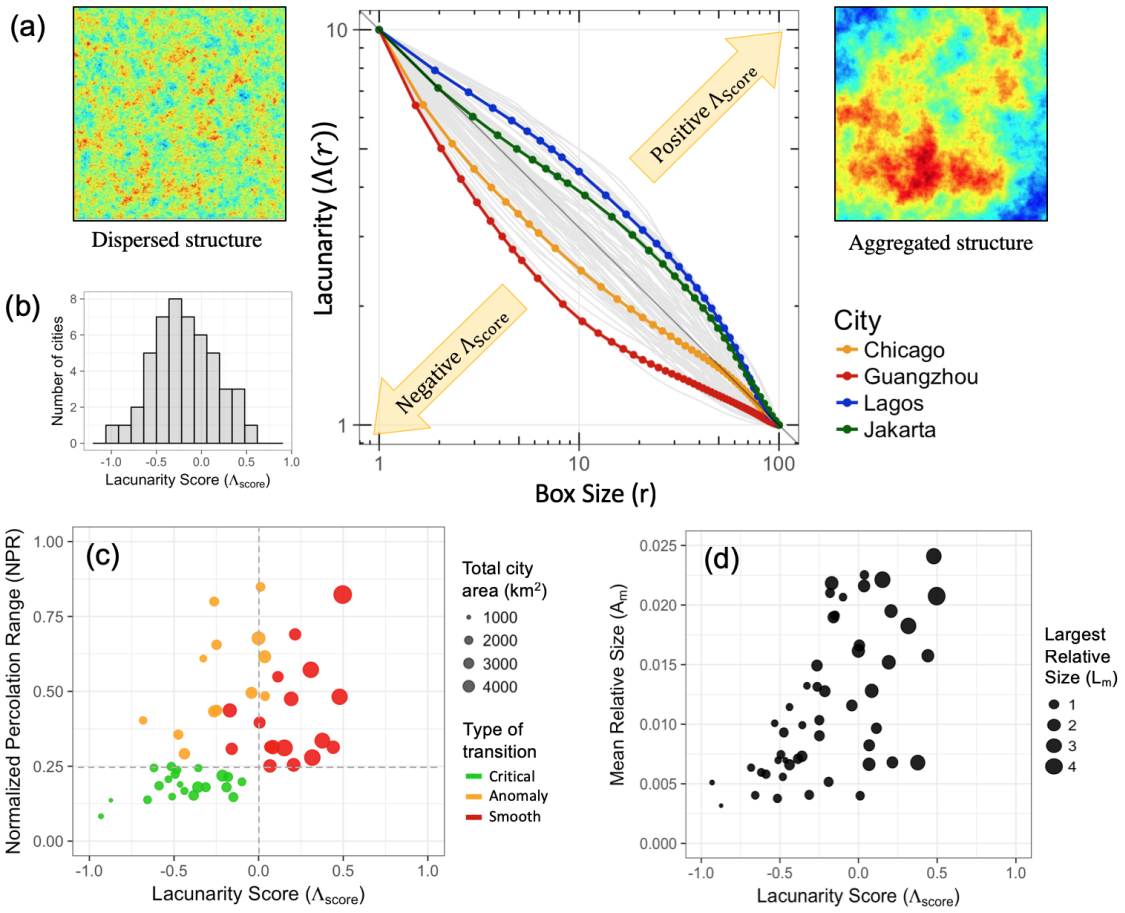

Figure 3: (a) Lacunarity curves of 49 cities (in grey) and the four archetype cities (in colour) shown on a $log(\Lambda)$ vs $log(r)$ plot. The cities with a concave downwards shape in the upper side of the diagonal indicate larger and more aggregated gaps, whereas cities underneath the curve indicate a more uniform dispersed pattern of islets and smaller gaps. (b) Histogram of Λ_{score} of 49 cities (mean = 0.04, s.d. = 0.38). (c) Scatter plot of percolation transition range and Lacunarity score. This figure illustrates the classification of cities into the 2 classes based on Lacunarity Score and the type of transition. (d) Scatter plot of Mean Relative Heat Islet Size (A_M) versus Λ_{score}. Additionally, since the islet-size distribution is heavy tailed, in addition to the A_M, the largest islet size (as a percentage of the total city area) is indicated using the marker size. The A_M and the largest-heat islet size (A_L) serve to illustrate the size distribution of the hottest islets occupying the ten percent of the city area.

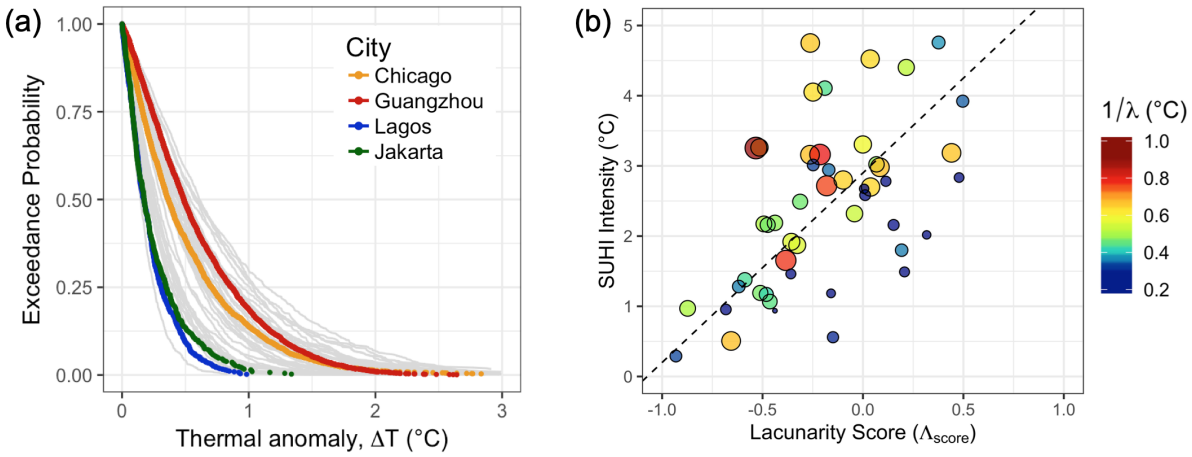

Figure 4: (a) Empirical pdf of ΔT for the 4 archetype cities shown on at their 90$^{\text{th}}$ percentile thermal thresholds respectively. The same for all 49 cities is shown in grey in the background. Each ΔT distribution was well described as an exponential distribution characterized by the parameter: λ. (b) Scatter plot of mean SUHI Intensity, defined as the difference between mean urban and rural temperatures, versus Lacunarity Score (Λ_{score}) is shown. A weak positive correlation ($R^2 = 0.344$) is detected shown as dashed regression line. The color as well as size of the marker indicates the inverse of rate parameter (λ) from Equation 4 which is equal to the mean Heat Islet Intensity for each distribution. Increasing size indicates higher temperatures within the heat islets.